Supplemental Document

Journal of the Optical Society of America A
OPTICS, IMAGE SCIENCE, AND VISION

Dual-constrained physics-enhanced untrained neural network for lensless imaging: supplement

ZEHUA WANG,[1] SHENGHAO ZHENG,[1] ZHIHUI DING,[1] AND CHENG GUO[2,*]

[1] *School of Instrumentation Science and Engineering, Harbin Institute of Technology, Harbin 150001, China*
[2] *Faculty of Computing, Harbin Institute of Technology, Harbin 150001, China*
[*] *guocheng_27@163.com*

Supplement DOI: https://doi.org/10.6084/m9.figshare.24796716

Parent Article DOI: https://doi.org/10.1364/JOSAA.510147

DPENet: a dual-constrained physics-enhanced untrained neural network for lensless maging: supplemental document

1. Gradient calculation

1.1 L_2 term

In this section we derive the gradient of L_2 term in Eq. (16). With the chain rule of matrix differentiation [1], the gradient can be expressed as

$$\begin{aligned}\nabla_{Q^{t-1}}\frac{1}{2}\left\|P^t-Q^{t-1}+S^{t-1}\right\|_2^2&=\left(\frac{\partial\frac{1}{2}\left\|P^t-Q^{t-1}+S^{t-1}\right\|_2^2}{\partial Q^{t-1}}\right)^{\mathrm{T}}\\&=\left(\frac{\partial\frac{1}{2}\left\|P^t-Q^{t-1}+S^{t-1}\right\|_2^2}{\partial P^t-Q^{t-1}+S^{t-1}}\cdot\frac{\partial P^t-Q^{t-1}+S^{t-1}}{\partial Q^{t-1}}\right)^{\mathrm{T}},\end{aligned}\tag{S1}$$

where $(\cdot)^{\mathrm{T}}$ is a transpose operator, and the derivatives are

$$\frac{\partial\frac{1}{2}\left\|P^t-Q^{t-1}+S^{t-1}\right\|_2^2}{\partial P^t-Q^{t-1}+S^{t-1}}=\left(P^t-Q^{t-1}+S^{t-1}\right)^{\mathrm{T}},\tag{S2}$$

$$\frac{\partial P^t-Q^{t-1}+S^{t-1}}{\partial Q^{t-1}}=-E.\tag{S3}$$

Thus, substituting Eq. (S2) and Eq. (S3) into Eq. (S1), the gradient is computed as

$$\begin{aligned}&\nabla_{Q^{t-1}}\frac{1}{2}\left\|P^t-Q^{t-1}+S^{t-1}\right\|_2^2\\&=\left[\left(P^t-Q^{t-1}+S^{t-1}\right)^{\mathrm{T}}\times-E\right]^{\mathrm{T}}\\&=-\left(P^t-Q^{t-1}+S^{t-1}\right).\end{aligned}\tag{S4}$$

1.2. Total variation term

For derivation convenience, we predefine some terms as follows

$$l_1=\left(\mathrm{D_x}\cdot Q^{t-1}\right)^2+\left(\mathrm{D_y}\cdot Q^{t-1}\right)^2+\varepsilon,\tag{S5}$$

$$l_2=\mathrm{D_x}\cdot Q^{t-1},\tag{S6}$$

$$l_3=\mathrm{D_y}\cdot Q^{t-1}.\tag{S7}$$

According to the chain rule of matrix differentiation [1], $\nabla_{Q^{t-1}}\mathrm{TV}\left(Q^{t-1}\right)$ can be expressed as

$$\begin{aligned}\nabla_{Q^{t-1}}\mathrm{TV}\left(Q^{t-1}\right)&=\left[\frac{\partial\mathrm{TV}\left(Q^{t-1}\right)}{\partial Q^{t-1}}\right]^{\mathrm{T}}\\&=\left[\frac{\partial\mathrm{TV}\left(Q^{t-1}\right)}{\partial l_1}\cdot\left(\frac{\partial l_1}{\partial l_2}\cdot\frac{\partial l_2}{\partial Q^{t-1}}+\frac{\partial l_1}{\partial l_3}\cdot\frac{\partial l_3}{\partial Q^{t-1}}\right)\right]^{\mathrm{T}},\end{aligned}\tag{S8}$$

where

$$\frac{\partial\mathrm{TV}\left(Q^{t-1}\right)}{\partial l_1}=\frac{\partial\sum\sqrt{l_1}}{\partial l_1}=\frac{1}{2}\left[\frac{1}{\sqrt{\left(\mathrm{D_x}\cdot Q^{t-1}\right)^2+\left(\mathrm{D_y}\cdot Q^{t-1}\right)^2+\varepsilon}}\right]^{\mathrm{T}},\tag{S9}$$

$$\frac{\partial l_1}{\partial l_2}=\frac{\partial\left(l_2\right)^2+\mathrm{const}}{\partial l_2}=2\mathrm{diag}\left(l_2\right),\tag{S10}$$

$$\frac{\partial l_1}{\partial l_3}=\frac{\partial\left(l_3\right)^2+\mathrm{const}}{\partial l_3}=2\mathrm{diag}\left(l_3\right),\tag{S11}$$

$$\frac{\partial l_2}{\partial Q^{t-1}}=\frac{\partial\mathrm{D_x}\cdot Q^{t-1}}{\partial Q^{t-1}}=\mathrm{D_x},\tag{S12}$$

$$\frac{\partial l_3}{\partial Q^{t-1}}=\frac{\partial\mathrm{D_y}\cdot Q^{t-1}}{\partial Q^{t-1}}=\mathrm{D_y}.\tag{S13}$$

The operator $\mathrm{diag}\left(\cdot\right)$ arranges the entries of a vector into the diagonal of a matrix. Thus, substituting Eqs. (S5)-(S7) and Eqs. (S9)-(S13) into Eq. (S8), the gradient is computed as

$$\begin{aligned}&\nabla_{Q^{t-1}}\mathrm{TV}\left(Q^{t-1}\right)\\&=\left[\frac{\partial\mathrm{TV}\left(Q^{t-1}\right)}{\partial l_1}\cdot\left(\frac{\partial l_1}{\partial l_2}\cdot\frac{\partial l_2}{\partial Q^{t-1}}+\frac{\partial l_1}{\partial l_3}\cdot\frac{\partial l_3}{\partial Q^{t-1}}\right)\right]^{\mathrm{T}}\\&=\left\{\frac{1}{2}\left[\frac{1}{\sqrt{\left(\mathrm{D_x}\cdot Q^{t-1}\right)^2+\left(\mathrm{D_y}\cdot Q^{t-1}\right)^2+\varepsilon}}\right]^{\mathrm{T}}\cdot\left[2\mathrm{diag}\left(\mathrm{D_x}\cdot Q^{t-1}\right)\cdot\mathrm{D_x}+2\mathrm{diag}\left(\mathrm{D_y}\cdot Q^{t-1}\right)\cdot\mathrm{D_y}\right]\right\}^{\mathrm{T}}\\&=\left[\left(\mathrm{D_x}\right)^{\mathrm{T}}\cdot\mathrm{diag}\left(\mathrm{D_x}\cdot Q^{t-1}\right)+\left(\mathrm{D_y}\right)^{\mathrm{T}}\cdot\mathrm{diag}\left(\mathrm{D_y}\cdot Q^{t-1}\right)\right]\cdot\frac{1}{\sqrt{\left(\mathrm{D_x}\cdot Q^{t-1}\right)^2+\left(\mathrm{D_y}\cdot Q^{t-1}\right)^2+\varepsilon}}\\&=-\left[\mathrm{D_x}\frac{\mathrm{D_x}\cdot Q^{t-1}}{\sqrt{\left(\mathrm{D_x}\cdot Q^{t-1}\right)^2+\left(\mathrm{D_y}\cdot Q^{t-1}\right)^2+\varepsilon}}+\mathrm{D_y}\frac{\mathrm{D_y}\cdot Q^{t-1}}{\sqrt{\left(\mathrm{D_x}\cdot Q^{t-1}\right)^2+\left(\mathrm{D_y}\cdot Q^{t-1}\right)^2+\varepsilon}}\right].\end{aligned}\tag{S14}$$

Notice that Eq. (S14) can be simplified using image gradient operator ∇ and divergence operator $\nabla\cdot$, we arrive at gradient as

$$\nabla_{Q^{t-1}}\mathrm{TV}\left(Q^{t-1}\right)=-\nabla\cdot\left[\frac{\nabla Q^{t-1}}{\sqrt{\left|\nabla Q^{t-1}\right|^2+\varepsilon}}\right]. \tag{S15}$$

1.3. Data fidelity term

In this section we derive the gradient of data fidelity term L_A^t with respect to A^{t-1}. For derivation convenience, let

$$o^{t-1}=A^{t-1}\odot\exp\left(\mathrm{i}P^t\right), \tag{S16}$$

$$u^{t-1}=H\cdot\left[A^{t-1}\odot\exp\left(\mathrm{i}P^t\right)\right], \tag{S17}$$

$$r^{t-1}=\left|H\cdot\left[A^{t-1}\odot\exp\left(\mathrm{i}P^t\right)\right]\right|-\sqrt{I}, \tag{S18}$$

where o^{t-1} is object's wavefield. u^{t-1} is the diffractive field at the observed plane. r^{t-1} denotes the residual amplitude component. Accordingly, the gradient $\nabla_{A^{t-1}}L_A^t$ can be expressed by the chain rule of complex matrix differentiation [2] as

$$\begin{aligned}\nabla_{A^{t-1}}L_A^t&=\left(\frac{\partial L_A^t}{\partial A^{t-1}}\right)^{\mathrm{T}}\\&=\left\{\frac{\partial L_A^t}{\partial r^{t-1}}\cdot\left[\frac{\partial r^{t-1}}{\partial u^{t-1}}\cdot\frac{\partial u^{t-1}}{\partial o^{t-1}}\cdot\frac{\partial o^{t-1}}{\partial A^{t-1}}+\frac{\partial r^{t-1}}{\partial\overline{u^{t-1}}}\cdot\frac{\partial\overline{u^{t-1}}}{\partial\overline{o^{t-1}}}\cdot\frac{\partial\overline{o^{t-1}}}{\partial A^{t-1}}\right]\right\}^{\mathrm{T}}\\&=\left\{2\left(r^{t-1}\right)^{\mathrm{T}}\cdot\left[\frac{\partial r^{t-1}}{\partial u^{t-1}}\cdot\frac{\partial u^{t-1}}{\partial o^{t-1}}\cdot\frac{\partial o^{t-1}}{\partial A^{t-1}}+\frac{\partial r^{t-1}}{\partial\overline{u^{t-1}}}\cdot\frac{\partial\overline{u^{t-1}}}{\partial\overline{o^{t-1}}}\cdot\frac{\partial\overline{o^{t-1}}}{\partial A^{t-1}}\right]\right\}^{\mathrm{T}},\end{aligned} \tag{S19}$$

where

$$\frac{\partial r^{t-1}}{\partial u^{t-1}}=\frac{\partial\left|u^{t-1}\right|-\sqrt{I}}{\partial u^{t-1}}=\mathrm{diag}\left(\frac{\overline{u^{t-1}}}{\left|u^{t-1}\right|}\right), \tag{S20}$$

$$\frac{\partial u^{t-1}}{\partial o^{t-1}}=\frac{\partial\left[H\cdot o^{t-1}\right]}{\partial o^{t-1}}=H, \tag{S21}$$

$$\frac{\partial o^{t-1}}{\partial A^{t-1}}=\frac{\partial\left[\exp\left(\mathrm{i}P^t\right)\odot A^{t-1}\right]}{\partial A^{t-1}}=\mathrm{diag}\left[\exp\left(\mathrm{i}P^t\right)\right], \tag{S22}$$

$$\frac{\partial r^{t-1}}{\partial\overline{u^{t-1}}}=\frac{\partial\left|u^{t-1}\right|-\sqrt{I}}{\partial\overline{u^{t-1}}}=\mathrm{diag}\left(\frac{u^{t-1}}{\left|u^{t-1}\right|}\right), \tag{S23}$$

$$\frac{\partial\overline{u^{t-1}}}{\partial\overline{o^{t-1}}}=\frac{\partial\left[\overline{H}\cdot\overline{o^{t-1}}\right]}{\partial\overline{o^{t-1}}}=\overline{H}, \tag{S24}$$

$$\frac{\partial\overline{o^{t-1}}}{\partial A^{t-1}}=\frac{\partial\left[\exp\left(-\mathrm{i}P^t\right)\odot A^{t-1}\right]}{\partial A^{t-1}}=\mathrm{diag}\left[\exp\left(-\mathrm{i}P^t\right)\right]. \tag{S25}$$

$\overline{(\cdot)}$ denotes conjugate operator. Thus, after Eqs. (S16)-(S18) and Eqs. (S20)-(S25) are plugged into Eq. (S19), the final closed-form of the gradient $\nabla_{A^{t-1}} L_A^t$ is derived as

$$
\begin{aligned}
&\nabla_{A^{t-1}} L_A^t \\
&= \left\{ 4\,\mathrm{Re}\left\{ \left(r^{t-1}\right)^{\mathrm{T}} \cdot \mathrm{diag}\left(\frac{u^{t-1}}{\left|u^{t-1}\right|} \right) \cdot \overline{H} \cdot \mathrm{diag}\left[\exp\left(-\mathrm{i}P^t\right) \right] \right\} \right\}^{\mathrm{T}} \\
&= 4\,\mathrm{Re}\left\{ A^{t-1} - \mathrm{diag}\left[\exp\left(-\mathrm{i}P^t\right) \right] \cdot H^* \cdot \mathrm{diag}\left(\frac{u^{t-1}}{\left|u^{t-1}\right|} \right) \cdot \sqrt{I} \right\} \\
&= 4\,\mathrm{Re}\left\{ A^{t-1} - \exp\left(-\mathrm{i}P^t\right) \odot \left\{ H^* \cdot \left\{ \sqrt{I} \odot \frac{H \cdot \left[A^{t-1} \odot \exp\left(\mathrm{i}P^t\right) \right]}{\left| H \cdot \left[A^{t-1} \odot \exp\left(\mathrm{i}P^t\right) \right] \right|} \right\} \right\} \right\}.
\end{aligned}
\tag{S26}
$$

2. Numerical simulation

2.1 Denoiser selection

In this section, we conduct the numerical simulation to select optimal denoiser for DPENet, and then investigate the generality and stability of our method. The grey-scaled biological tissue images captured from a commercial microscope (Olympus, IX71) are used for ground truth. The simulated parameters are listed as follows: (1) the amplitude image of the object is a grey-scale image and its phase is set as a constant value; (2) the sampling size of the diffraction field is 512×512; (3) the wavelength is 532nm; (4) the sample-to-detector distance is 3.46 mm; (5) iterative number is 10000. The captured intensity pattern serves as the input of PhysenNet and DPENet for reconstruction. The structural similarity index measure (SSIM) [3] is selected as a metric to quantitatively evaluate the reconstruction performance of different methods. Gaussian noise with a variance of $\sigma = 5$ is added in the intensity pattern to examine the imaging performance.

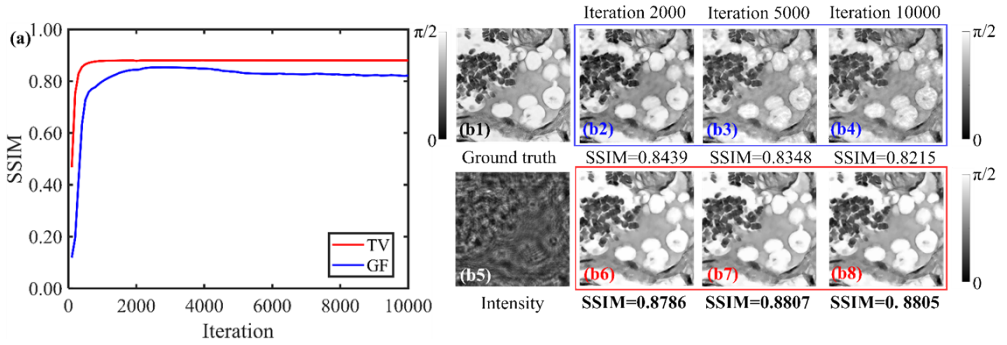

Fig. S1. Numerical simulation results using different denoisers. (a) Convergence curves. (b1) Ground truth phase image. (b5) Diffraction pattern. (b2)-(b4) and (b6)-(b8) are retrieved phase images of guided filter and total variation for 2000 iterations, 5000 iterations and 10000 iterations.

The regularization term in Eq. (5) is used to preserve high-frequency information while denoising. Here we consider guide filter (GF) [4] and total variation (TV) [5] to find an optimal denoiser. The reconstructed images using different denoisers are shown in Fig. S1. It is noted that total variation gets the higher metric values and realizes more stable reconstruction than guided filter. In addition, the retrieved results in Figs. S1(b2-b4) and Figs. S1(b6-b8) are

consistent with their SSIM curves. Total variation removes the background noise compared with guided filter.

We also test the image generality by comparing the two denoisers in different noise levels ($\sigma = 5, \sigma = 10$) on other microscopic images. The images are shown in Fig. S2. The quantitative results are given in Tab. S1 and bolded fonts represent higher SSIM values (10000 iterations), where total variation provides better results in all simulated images. In conclusion, we use total variation as a regularized term for denoising.

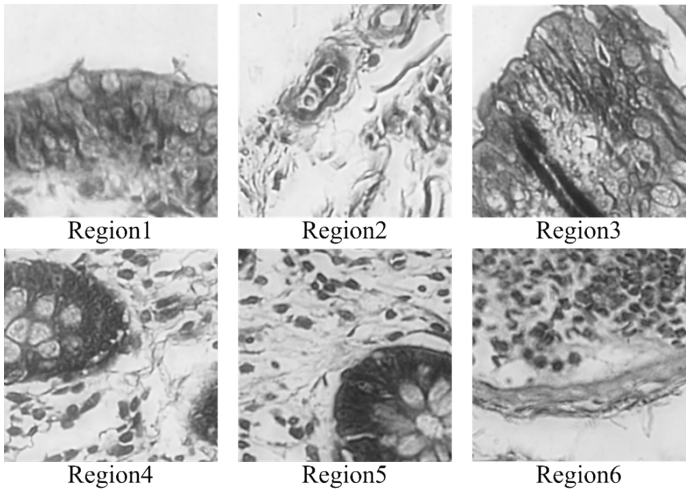

Fig. S2. Microscopic images used in simulation.

Table. S1 SSIM results of denoisers under different noise conditions ($\sigma = 5$, $\sigma = 10$).

$\sigma = 5$	Region1	Region2	Region3	Region4	Region5	Region6
GF	0.9010	0.8867	0.8633	0.8129	0.8546	0.8381
TV	**0.9116**	**0.9152**	**0.8689**	**0.8791**	**0.8710**	**0.8912**
$\sigma = 10$	Region1	Region2	Region3	Region4	Region5	Region6
GF	0.8369	0.8247	0.7967	0.7814	0.7616	0.7764
TV	**0.8599**	**0.8592**	**0.8053**	**0.8257**	**0.8165**	**0.8486**

2.2 Method comparison

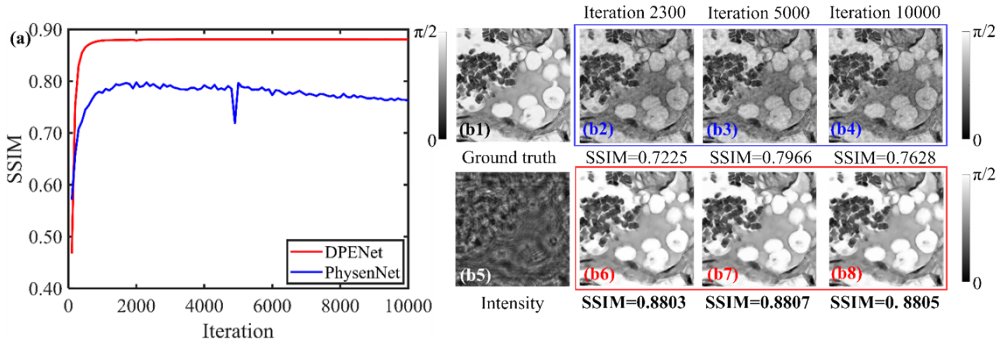

Fig. S3. Numerical simulation results of different algorithms. (a) Convergence curves. (b1) Ground truth phase image. (b5) Diffraction pattern. (b2)-(b4) and (b6)-(b8) are retrieved phase images of PhysenNet and our method for 2300 iterations, 5000 iterations and 10000 iterations.

We compare the two methods on a microscopic image in Fig. S3. In Fig. S3. (a), the SSIM values of PhysenNet reaches its peak at 2300 iterations and then drops in the rest of iterations, while the SSIM of DPENet dramatically increases within 1000 iterations and then almost keeps at the same level. The retrieved results in Figs. S3(b2-b4) and Figs. S3(b6-b8) are consistent with their SSIM curves. DPENet can wipe out the noisy artifacts and finally reach at a higher SSIM level by contrast with PhysenNet. These results indicate that DPENet is more noise-robust than PhysenNet.

We also test the image generality by comparing the two methods in different noise levels ($\sigma = 5, \sigma = 10$) on other microscopic images. The quantitative results in Tab. S2 demonstrate that our method surpasses PhysenNet in all simulated images. Numerical simulation results prove that DPENet has greater noise-robustness and image generality than PhysenNet.

Table. S2 SSIM results of PhysenNet and DPENet under different noise conditions ($\sigma = 5$, $\sigma = 10$).

$\sigma = 5$	Region1	Region2	Region3	Region4	Region5	Region6
PhysenNet	0.7840	0.7844	0.8052	0.8020	0.7903	0.8187
DPENet	**0.9116**	**0.9152**	**0.8689**	**0.8791**	**0.8710**	**0.8912**
$\sigma = 10$	Region1	Region2	Region3	Region4	Region5	Region6
PhysenNet	0.6054	0.6897	0.6524	0.6631	0.6523	0.6925
DPENet	**0.8599**	**0.8592**	**0.8053**	**0.8257**	**0.8165**	**0.8486**

References

1. G. Strang, “Introduction to linear algebra,” Wellesley-Cambridge Press (2022).
2. E. J. Candes, X. Li, and M. Soltanolkotabi, “Phase retrieval via Wirtinger flow: Theory and algorithms,” IEEE Transactions on Information Theory 61, 1985-2007 (2015).
3. Z. Wang, A. C. Bovik, H. R. Sheikh, and E. P. Simoncelli, “Image quality assessment: from error visibility to structural similarity,” IEEE transactions on image processing 13, 600-612 (2004).
4. K. He, J. Sun, and X. Tang, “Guided image filtering,” IEEE transactions on pattern analysis and machine intelligence 35, 1397-1409 (2012).
5. Y. Chi and S. H. Chan, “Fast and robust recursive filter for image denoising,” in 2018 IEEE international conference on acoustics, speech and signal processing (ICASSP), 1708-1712 (2018).